

# Automation of quantitative muscle cell analysis by image segmentation

Zdenka Uhríková\*

Faculty of Mathematics, Physics and Informatics,  
Comenius University, Bratislava, Slovakia

## Abstract

In this paper we describe a new approach to quantitative measurements on muscle cell images. Our algorithm processes gray scaled images obtained from electron microscopy (12000× magnification). By means of discrete Fourier transform we detect the orientation of muscle fibers. Afterwards, applying our thresholding method, we detect boundaries between constituents of myofibrils (A band, I band and Z line). From these boundaries we estimate lengths of each myofibril constituent, since these lengths define the type of a muscle cell. Finally, we compare data measured by our algorithm, with data estimated manually.

**Keywords:** muscle cell, segmentation, morphometry

## 1 Introduction

Recovery of geometric shapes from images of biological objects represent a challenging as well as complicated theme in Computer Vision.

According to electron microscopic (EM) studies of muscle cells, there is a need to define muscle cell characteristics from EM images. With respect to the stereological and morphometric measurements, image processing methods are mainly based on manual processing [2].

Previously much effort has been spent on developing general image processing algorithms, however development of algorithms suitable for microscopic images has been neglected. Recently, just several algorithms were proposed to solve specific problems in muscle cell morphometry.

For purpose of a diagnosis of neuromuscular diseases, Dryden et al. [1] studied cross-sectional images of muscle cells. They proposed to apply Bayesian method for the segmentation of muscle fibre images approximated by a Dirichlet tessellation. The segmented image is represented by Voronoi polygons, where a single Voronoi polygon corresponds to a single fiber.

According to studies of muscle cell mitochondria, electron microscopy images of longitudinal sections are often used. Guo et al. [4] proposed an automated algorithm

for mitochondria detection, based on application of a two-dimensional matched filter to trace the borders of mitochondria. Vendelin et al. [11] found that mitochondria are arranged in crystal-like patterns and they also evaluated distances between pairs of mitochondria. In fact, both [4] and [11] analyze only spot-shaped mitochondria, and neglected long ones.

In the field of image processing, several applications were developed that simplify morphometrical measurements, and also attempt to aim at their automatization. Today, numerous image processing tools exist for different applications. In most cases, they are oriented on 3D visualization and often have high requirements on hardware. Additionally they can be efficiently used on very specific types of images.

One of the powerful tool is the open source project *ImageJ* [7], an image processing toolkit written in Java. It runs on any platform, supports many file formats and allows to write user-specified macros and plugins. It provides standard image processing functions, geometric transformations and image statistics.

Another powerful image processing tool is *analySIS* from Soft Imaging System [9]. It is a commercial product with plenty of automatic and manual processing features.

*Ellipse* [10] is an image analysis tool that allows drawing and editing of images, manual and interactive segmentation and further calculations of parameters such as the area and the perimeter of desired image objects.

All mentioned systems provide image processing functions for universal application, but do not offer the required specific functions for morphometric muscle cell analysis.

## 2 Muscle cell morphology

Muscles are divided into three basic types according to their structure: striated, cardiac and smooth muscles. With respect to the user requirements this work is oriented to skeletal muscles.

The basic unit of skeletal muscle is the muscle cell—fiber (Figure 1), which is a multinucleated cell tightly surrounded by a surface membrane—sarcolemma. It consists of organelles, from which myofibrils, mitochondria, t-tubules and sarcoplasmatic reticulum are the most important ones.

\*e-mail: zdenka.uhrikova@gmail.com

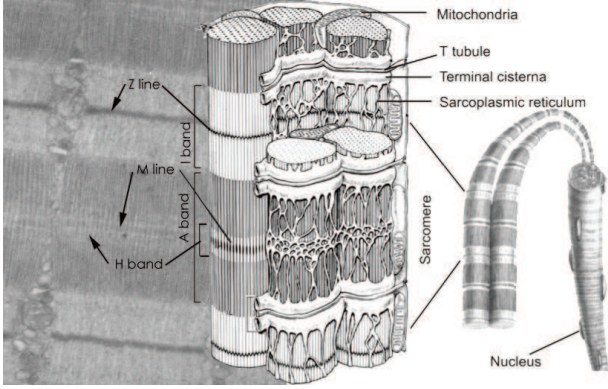


Figure 1: Muscle fiber. Original illustration taken from <http://herkules.oulu.fi/isbn9514271521/html/x451.html>

Myofibrils are thin and long contractile fibres, organized in parallel bundles, spanning the whole length of the cell. They are longitudinally divided into A band, I band and Z line, which show the striated pattern under the microscope. More than 50% of the muscle cell volume is occupied by myofibrils.

Each myofibril is made up of bunch of parallel filaments. The thick filaments have a diameter of about 15 nm. They are composed of the protein myosin and produce the dark A band. The A bands are bisected by the H zone. The H zone is that portion of the A band where the thick and thin filaments do not overlap. The thin filaments have a diameter of about 5 nm and they create the light I band. I bands are bisected by Z lines.

The thick and thin filaments create a bundle which can be separated into repeated patterns—sarcomere. Sarcomere is defined as the segment between two Z lines.

Mitochondria are membrane enclosed organelles of irregular smooth shape and variable size. Mitochondria are in skeletal muscles either arranged in pairs on both sides of the Z line or form columns in the longitudinal direction in the interfilament space [5]. Mitochondria, depending on the cell type, take 5–40% of the muscle cell volume.

Sarcoplasmic reticulum is membranous structure consisting of terminal cisterns that are closely related to the T-tubules. T-tubules are long and thin tubes formed from sarcolemma. They form a network around myofibrils, perpendicular to the cell surface.

### 3 Automatic analysis of muscle cells

Morphometry represents an important category of cell analysis tools and comprises methods of extracting quantitative objects characteristics from shapes. Morphometry enables to quantitatively characterize biological 'forms' of interest, which in our case are muscle cell organelles. Especially, we are interested in computation of lengths of sarcomere and its constituents (A band, I band and Z line). These lengths help in characterizing the muscle type and

revealing adaptational changes at the level of contractile filaments [3].

According to these requirements we implemented an automatic image processing tool which encapsulates segmentation of these three myofibril constituents.

It processes gray scale longitudinal sections images of about  $1500 \times 2000$  pixels in three steps:

- Detect the longitudinal direction of a fiber
- Detection of region boundaries in the image, and
- Measurement of sarcomere, A band and Z line lengths

#### 3.1 Estimation of the longitudinal direction

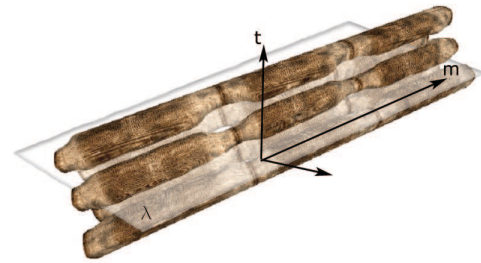


Figure 2: A muscle fiber model obtained from [6].  $m$  - main axis of fiber,  $t$  - transversal axis,  $\lambda$  - longitudinal section of muscle

The longitudinal direction is defined by a main axis of the fiber (see Figure 2), i.e., by the orientation of myofibrils. With respect to the fact that myofibrils take the most part of the image, we can extract this longitudinal direction automatically. Following the noticeable periodicity of thin filaments in a given image (Figure 3a), it is suitable to use two dimensional discrete Fourier transform (DFT) (Figure 3b) to detect this direction.

Using point by point conjugate multiplication of image in frequency domain, we achieve better sharpening of direction in an image. Consequently we apply inverse DFT.

The resulting image now includes only a few parallel stripes in the longitudinal direction, and, moreover, one of them certainly passes through the center of image (according to the centricity attribute of DFT). We use the convolution mask (the matrix 1) to make the resultant image clearer (Figure 3c).

$$\begin{pmatrix} -1 & -1 & -1 & -1 & -1 \\ -1 & -1 & 24 & -1 & -1 \\ -1 & -1 & -1 & -1 & -1 \\ -1 & -1 & -1 & -1 & -1 \end{pmatrix} \quad (1)$$

The longitudinal direction is defined by a line passing through the center of such modified image. We find the equation for the central line by searching two end-points  $A$  and  $B$  of the desired line (Figure 3d). Starting in the center

of the image we follow the high intensity points in both directions (up and down) as long as the intensity is above a specified threshold value.

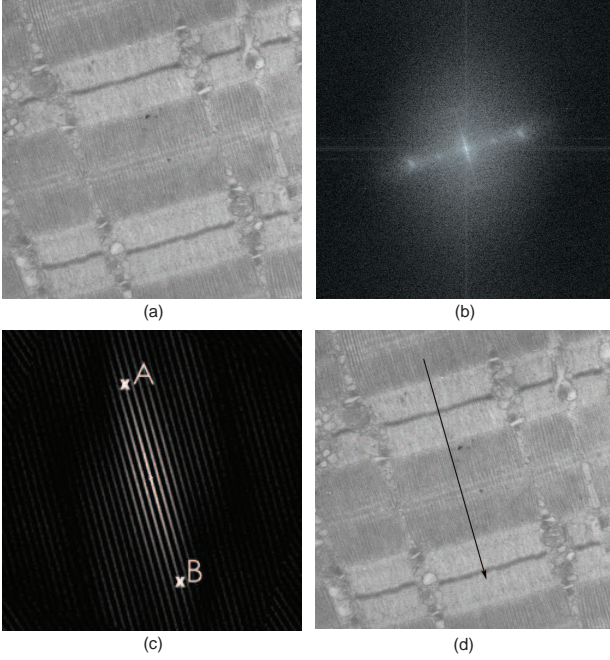


Figure 3: Direction detection. (a) The original image. (b) Fourier transform of the image in (a). (c) After squaring, inverse transform and applying the convolution mask. (d) Detection of longitudinal direction.

### 3.2 Mask based thresholding

A frequently used technique for image segmentation is an operation of thresholding. Thresholding is a non-linear operation that converts a gray-scale image into a binary image where the two levels are assigned to pixels that are below and above the specified threshold value. We modify the basic thresholding scheme by computing a mean value in a neighborhood defined by a mask. From the statistical distribution of intensities in our sets of images we found out that the mean image intensity is a suitable threshold value to segment the given image in light (I band) and dark zones (A band and Z line). The image mean  $\bar{m}$  intensity is as follows:

$$\bar{m} = \frac{1}{wh} \sum_{i=0}^w \sum_{j=0}^h x_{ij} \quad (2)$$

where  $w$  and  $h$  are width and height of the image.

We introduce five types of masks ( $M_1, M_2, M_3, M_4, M_5$ ) with dimensions equal to  $M_1 = 26 \times 26$ ,  $M_2 = 28 \times 28$ ,  $M_3 = 30 \times 30$ ,  $M_4 = 32 \times 32$ ,  $M_5 = 34 \times 34$  points.

For each image point  $I_{ij}$  we estimate all 5 mean intensities  $m_{ij}^k$ ,  $k = 1, \dots, 5$  corresponding to each of these masks. By comparing to the mean  $\bar{m}$  we get a three-level (yellow,

red, green) thresholded image  $T$  (Figure 4) where:

$$T_{ij} = \begin{cases} \text{yellow} & \text{if } \exists k : m_{ij}^k = \bar{m} \\ \text{red} & \text{else if at least 3 } m_{ij}^k \text{ are less than } \bar{m} \\ \text{green} & \text{else if at least 3 } m_{ij}^k \text{ are more than } \bar{m} \end{cases}$$

By means of the standard deviation we define the 'threshold step' to obtain more iso-levels derived from the threshold value (Figure 4b).

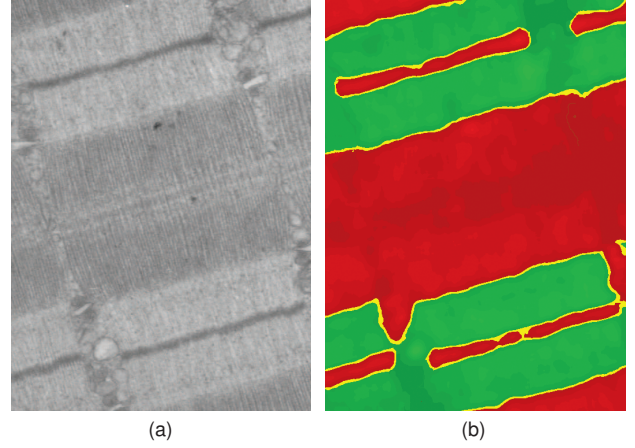


Figure 4: Thresholding. (a) The original image. (b) The thresholded image. Using the threshold step: the more levels are in red color the more levels are also in green color.

### 3.3 Boundaries

#### 3.3.1 Boundary detection

There are significant transversal boundaries between Z line and I band, and A band and I band. We find them by traversing the thresholded image in the longitudinal direction, using only areas equal to  $\bar{m}$  (yellow parts). Each time we detect beginning of yellow region and its corresponding end (still in a longitudinal direction), we mark up its center. These mark up points create a point skeleton, from which we clean up isolated points with no neighbors. The remaining points create boundaries. The result is on the Figure 5a.

#### 3.3.2 Length estimation

Lengths of sarcomere constituents are measured in a longitudinal direction. Unfortunately, we do not have any knowledge about sarcomere lengths in a given image, therefore we need some orientation values from which we could start from.

By evaluating distances between two boundaries in longitudinal direction (over the darker part in thresholded image) we obtain a bimodal histogram (Figure 5c). From the sarcomere layout we know that its first peak belongs to the Z line and the second to the A band.

In some cases we can get trimodal histogram, nevertheless it depends on the image type and quality. In this case, the first peak belongs to the Z line, second to half of the A band (from one boundary to beginning of H band) and last one belongs to the A band.

### 3.3.3 Differentiate boundaries

In this step we differentiate boundaries by assigning them to the Z lines and the A bands. Pairs of boundaries with the distance equal to the value of the first peak ( $\pm 10\%$ ) are Z line boundaries, and pairs of boundaries with the distance equal to the value of the second peak ( $\pm 10\%$ ) are A band boundaries. (Figure 5b).

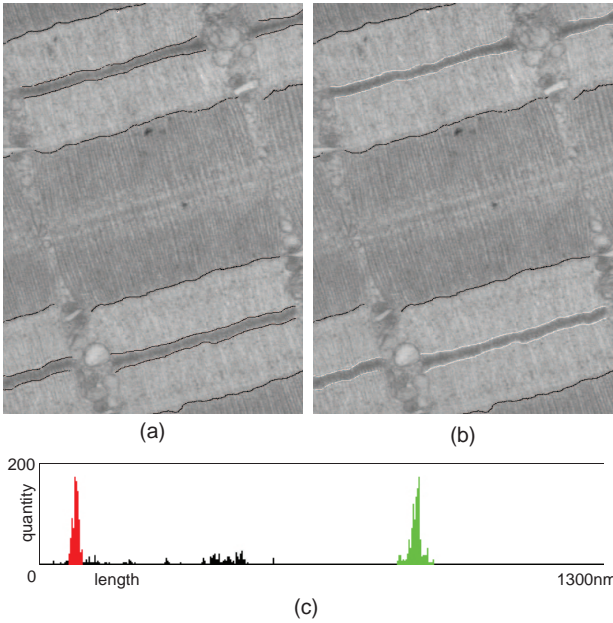


Figure 5: (a) Transversal boundaries. (b) Boundaries belonging to Z line (white) and A band (black). (c) Bimodal histogram of boundaries distances.

### 3.4 Quantitative analysis

The required length estimation is demonstrated in figure 6a.

A band length is the distance between two boundaries that belong to the same A band. The distance is measured in a longitudinal direction. To be sure that we measure the A band, we check if all measured lengths lie above the darker (A band) part of the thresholded image. Visualization of various A band lengths is depicted in Figure 6b.

The area between two detected Z line boundaries is Z line. We check whether the detected boundary goes close to the real boundary, and if not we shift the boundary by the threshold step in a longitudinal direction. The results of Z line lengths can be seen on Figure 6b.

The sarcomere goes from the one Z line to the second Z line. Measurement of the length of sarcomere is almost

the same like A band. We just check the first Z line, then the sequence of I-A-I bands and finally the second Z line (Figure 6c).

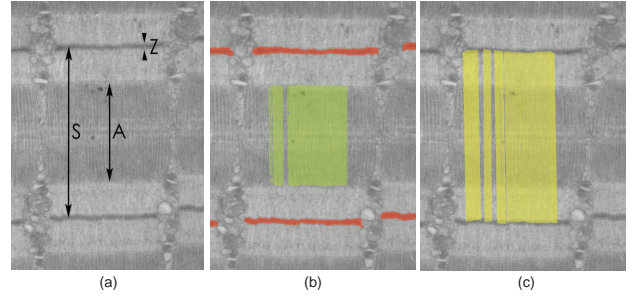


Figure 6: Length measurement. (a) S - length of sarcomere, A - length of A band, Z - length of Z line. (b) Measured length of A band and Z line. (c) Measured lengths of sarcomere.

## 4 Results

For testing purposes, we processed two sets of images from two different muscle cell types. The first set consists of 10 images (01–10), the second counts 5 images (11–15).

On average, in a given image we took over 200 measurements of A band, about 500 measurements of sarcomere and over 800 measurements of Z line, from which we computed an average and a corresponding standard deviation. The whole processing on a given image takes approximately 12 seconds.<sup>1</sup> Results are shown in table 1.

Set 1	$l_S \pm \sigma_S$	$n$	$l_A \pm \sigma_A$	$n$	$l_Z \pm \sigma_Z$	$n$
01	1673±33	953	1027±15	130	40±6	937
02	1634±23	527	1010±30	72	39±7	687
03	1796±9	302	1032±14	239	47±7	910
04	1452±13	476	968±15	342	37±6	799
05	1439±12	397	964±12	316	37±6	1108
06	1499±19	740	964±16	237	37±6	1358
07	1606±26	842	1003±16	60	37±6	1296
08	1587±14	967	1018±17	274	39±7	668
09	1645±5	59	964±15	555	37±6	784
10	1452±20	1021	946±13	470	36±5	873
Set 2	$l_S \pm \sigma_S$	$n$	$l_A \pm \sigma_A$	$n$	$l_Z \pm \sigma_Z$	$n$
11	2974±52	88	1205±25	113	78±9	310
12	3003±53	378	1220±24	66	82±13	638
13	3180±26	229	1260±21	388	88±12	949
14	3029±47	304	1221±22	299	88±10	952
15	3065±2	161	1211±17	190	82±14	497

Table 1: Results are evaluated in nanometers, conversion from image discrete space is 1 point = 3.5nm.  $l_S$  - length of sarcomere,  $l_A$  - length of A band,  $l_Z$  - length of Z line.  $\sigma$  - standard deviation,  $n$  - number of taken measurements.

<sup>1</sup>Using configuration Athlon 1600+, 1.4Ghz, 512MB RAM.

Manual measurement consisted of 5 measured values of sarcomere, A band and Z line in a given image. Original survey was done totally on 10 animals, five animals were healthy and five were with blocked expression of mitochondrial and cytosolic creatin-kinase ( $CK_{-/-}$ ) [8]. Twenty images were taken from a single animal, average values from healthy and defected animals were compared using paired Students t-test.

#### 4.1 Comparative analysis

We compared values from two aforementioned sets of images. Table 2 shows average of manual and automatic (by our algorithm) measurements compared by paired Students t-test. Probability  $P$  defines the degree of equivalence, e.g.  $P = 0$  stands for no equivalence and  $P = 1$  for identical sets.<sup>2</sup>

Set 1	$L_m[nm]$	$L_a[nm]$	$\Delta_L$	$P$
Sarcomere	1580	1578	-2	0.608
A band	992	989	-3	0.567
Z line	39	39	0	0.565

Set 2	$L_m[nm]$	$L_a[nm]$	$\Delta_L$	$P$
Sarcomere	3049	3050	+1	0.964
A band	1222	1223	+1	0.801
Z line	84	84	0	0.688

Table 2: Comparing values using paired Students t-test.  $L_m$  - average of manual processing,  $L_a$  - average of automatic processing,  $\Delta_L$  - difference  $L_a - L_m$ ,  $P$  - the probability of result, assuming the null hypothesis

## 5 Discussion

The advantage of the automatical processing in comparison with manual processing is in possibility making much more measured values per a single image. According to statistical analysis of more than 500 measured values of sarcomere and over 200 measured values of A band there is smaller probability of the error, and the results are more representative.

On average, our results differ 2 nanometers from manually obtained values, in an image discrete space it is less than a single pixel. Student's t-test indicates that the two measurements are not statistically significantly different.

Differences between average results from manual and automatic processing are caused mainly by insufficient number of tested images and different number of measurements performed on a single image. There are some problems when we detect a sarcomere beginning, but the corresponding end is not visible. This happens if the end of sarcomere is below or above our section, so it couldn't

<sup>2</sup> $P$  should be over 0.05 to be not significantly different

be covered in a image. Subsequently it may lead to incorrectly measured length of this sarcomere. These images must be then manually skipped. Other problems, e.g. the incorrect section orientation, are solved previously in the process of an image generation by biologists.

## 6 Conclusions and future work

In this paper we presented a system for automatic measurement of quantitative data in images of muscle cells. We detect the longitudinal direction of muscle fibers, which is important also for stereological measurements. Thresholding brings us closer to the segmentation of image, we have detected Z line and partly A band. Automatization of measurement of the lengths of sarcomere, A band and Z line gave us hundreds of measured values. Our results are the same to those obtained manually as estimated by statistical analysis.

A next step will be optimization of the segmentation, especially detection of mitochondria. Afterwards, we intend to automate stereological measuring. A further possibility to improve segmentation of our images is incorporation of the extended watershed transform—hierarchical watershed transform invented by Šrámek and Dimitrov [12], which is less sensitive to noise and, in contrary to thresholding, does not require threshold specification. Further, there is also a possibility of creating 3D models from such segmented images, following the work of Parulek et al. [6], if a series of fiber sections is available.

## 7 Acknowledgements

I would like to thank my supervisor Július Parulek for his useful ideas and help with this paper. Thanks go also to Ivan Zahradník for discussion of the problems, Miloš Šrámek for giving the finishing touches and to Laboratory of Cell Morphology (Marta Novotová and Lucia Tylková) at the Institute of Molecular Genetics and Physiology, SAS, for consultations and generals providing of muscle cell images. This work was supported by VEGA-2/6079/26.

## References

- [1] Ian L. Dryden, Rahman Farnoosh, and Charles C. Taylor. Image segmentation using voronoi polygons and mcmc, with application to muscle fibre images.
- [2] Brenda R. Eisenberg, Aileen M. Kuda, and James B. Peter. Stereological analysis of mammalian skeletal muscle. *The Journal Of Cell Biology*, 60:732–754, 1974.
- [3] L. Tylková et al. New frontiers in cardiovascular research. page 35, 2004.

- [4] Yu Guo, Biao Gong, Sebrina Levesque, Thomas Manfredi, and Ying Sun. Automated detection and delineation of mitochondria in electron micrographs of human skeletal muscles. *Microscopy Research and Technique*, 63:133–139, 2004.
- [5] T. Ogata and Y. Yamasaki. Ultra-high-resolution scanning electron microscopy of mitochondria and sarcoplasmic reticulum arrangement in human red, white and intermediate muscle fibers. *Cell Tissue Res*, 241:251–256, 1985.
- [6] Július Parulek, Ivan Zahradník, and Miloš Šrámek. A modelling tool for construction of 3d structure of muscle cells. In J. Jan, J. Kozumplik, and I. Provaznik, editors, *Analysis of Biomedical Signals and Image proceedings*, pages 267–269, Brno University of Technology, Czech Republic, 2004.
- [7] Wayne Rasband. Imagej. <http://rsb.info.nih.gov/ij>.
- [8] K. Steeghs, F. Oerlemans, A. De Haan, A. Heerschap, L. Verdoodt, M. De Bie, W. Ruitenbeek, W. A. Benders, C. Jost, J. Van Deursen, P. Tullson, R. Terjung, P. Jap, W. Jacob, D. Pette, and B. D. Wieringa. Cytoarchitectural and metabolic adaptations in muscles with mitochondrial and cytosolic creatin kinase deficiencies. *Mol Cell Biochem*, 184:183–194, 1998.
- [9] Soft Imaging System. analysis. <http://www.soft-imaging.net/>.
- [10] ViDiTo Systems. Ellipse. <http://www.ellipse.sk>.
- [11] Marko Vendelin, Nathalie Beraud, Karen Guerrero, tatiana Andrienke, Andrey V. Kuznetsov, Jose Olivares, Laurence Kay, and Valdur A. Saks. Mitochondrial regular arrangement in muscle cells: a 'crystal-like' pattern. *Am J Physiol Cell Physiol*, 288:757–767, 2005.
- [12] M. Šrámek and L. I. Dimitrov. Segmentation of tomographic data by hierarchical watershed transform. *Journal of Medical Informatics and Technologies*, 3:MI–161–MI–169, 2002.